Improved elevated-temperature properties in Al-13%Si piston alloys by Mo addition

L. Jin, K. Liu*, X. -G. Chen

Department of Applied Sciences, University of Québec at Chicoutimi

(*Corresponding author: kun.liu@uqac.ca; Tel.: 1-4185455011 ext.7112; Fax: 1-4185455012)

Abstract

Eutectic Al-13%Si alloys are widely used in the automotive industry for manufacturing components, such as pistons and cylinder heads. To reduce greenhouse gas emissions and enhance the engine efficiency, their service temperature keeps increasing to 250–350 °C, leading to the deterioration of their mechanical properties and the creep resistance. In the present work, Mo was further added to Mn-containing Al-13%Si piston alloys aiming at improving the overall properties at elevated temperatures. Compared with the Mn-containing base alloy, Mo further enhanced the precipitation of dispersoids by expanding the dispersoid zone and restricting the dispersoid-free zone after the proper precipitation treatment (520 °C/12 h), resulting in a remarkable improvement in the yield strength at both room temperature and 300 °C, as well as the creep resistance at 300 °C. Furthermore, the beneficial effect of Mo addition on the improved yield strength and creep resistance was especially prominent during long-term thermal exposure (up to 1000 h at 300 °C) due to the synergistic effect of thermally stable dispersoids and the retardation of the gradual fragmentation and spheroidization of Si particles.

Keywords: Al-13%Si piston alloy; Mo; dispersoids; elevated-temperature properties; thermal stability

Introduction

Al-13%Si alloys are widely used in automotive components, such as cylinder heads and pistons, due to their high strength, excellent wear resistance, and low thermal expansion [1, 2]. Typical working temperatures for a diesel engine in the modern automotive industry can reach up to 250–350 °C due to the trends in engine design of reducing greenhouse gas emissions and enhancing engine efficiency [3, 4]. Therefore, the elevated-temperature properties are one of the most critical considerations in the design of piston materials [5].

Until now, the improvement in the elevated-temperature properties of Al-13%Si piston alloys has been predominately achieved via the addition of aluminide-forming elements, such as Fe [6, 7], Ni [8, 9], and Cu [9, 10] to produce a large volume of various intermetallics during solidification, which are thermally stable and can establish rigid networks with Si particles to strengthen the material. It has been reported that the elevated-temperature strength was significantly improved via Ni addition to form a

highly interconnected 3-D structure with 20 vol.% eutectic Si, Al_9FeNi, and $Al_{15}(Mn,Fe)_3Si_2$ aluminides [10]. However, while the Si network is one of the most striking features of eutectic Al-Si piston alloys [11, 12], their fragmentation and spheroidization at elevated temperatures is almost inevitable [13, 14], leading to the gradual destruction of the interconnected network during long service periods at elevated temperature and then deteriorating the elevated-temperature properties [6]. Therefore, maintaining the interconnected and rigid network between Si and other aluminides is necessary for piston alloys to retain their elevated-temperature properties.

Besides the introduce of a large quantity of thermally stable intermetallics to form the interconnected network in piston alloys, the strengthening of the α-Al matrix also plays an important role in improving their elevated-temperature properties. Meanwhile, dispersoid strengthening has been reported as one of most efficient methods to improve the strength of the aluminum matrix at elevated temperatures via precipitation of thermally stable dispersoids after appropriate heat treatment [15] with various alloying elements [16–20]. A similar trial was nbenpreliminarily performed in Al-13%Si piston alloys by Mn addition, and a reasonable improvement in the both strength and creep resistance was achieved by the introduction of dispersoids [3]. However, the evolution of elevated-temperature properties during the service period was rarely studied in the literature, which is one of most significant concerns in the selection of piston materials.

Furthermore, Mo has been reported to promote the formation of dispersoid and reduce the dispersoid-free zone (DFZ) in Al-Si cast alloys [18] and 3xxx alloys [21, 22], thereby significantly improving the elevated-temperature properties. In addition, it is also reported that Mo can further increase the critical thermal-stable temperature of dispersoids from 300 to 350 °C, even to 400 °C [21, 22], making it one of most potential additions to strengthen materials at elevated temperatures. However, research on alloying Mo with eutectic Al-13%Si alloy, in particular its effect on the elevated temperature properties, is limited.

In the present work, the precipitation of dispersoids by various Mo additions into a Mn-containing Al-13%Si piston alloy was studied by characterization of the dispersoid zone and dispersoid-free zone (DFZ) during heat treatment using an optical microscope (OM), scanning electron microscope (SEM), and transmission electron microscope (TEM). The influence of dispersoids on the yield strength and creep resistance at 300 °C was further investigated. Moreover, the evolution of the elevated-temperature properties (strength and creep resistance) during the prolonged thermal exposure at 300 °C for up to 1000 h was studied to evaluate the service life of the experimental alloys under simulated work conditions at elevated temperature.

Experimental

Four experimental Al-13%Si alloys with various Mo contents (0 to 0.40 wt.%) were designed and their chemical compositions analyzed with an optical emission spectrometer are shown in Table 1. In

each test, approximately 3.2 kg of material was prepared in a clay-graphite crucible using an electric resistance furnace. The melt was maintained at approximately 750 °C for 30 min and then degassed for 15 min before being poured into a permanent mold preheated to 250 °C. Finally, four 30×40×80 mm ingots were cast for the following experiments.

Table 1 Chemical composition of experimental alloys

Alloy #	Element, wt. %								
	Si	Cu	Mg	Ni	Fe	Mn	P	Mo	Al
B0	12.72	1.06	1.05	1.09	0.41	0.35	0.001	0	Bal.
B1	13.27	1.07	1.01	1.11	0.4	0.3	0.001	**0.15**	Bal.
B2	13.65	1.04	1.07	1.06	0.49	0.32	0.001	**0.25**	Bal.
B3	13.13	1.06	1.01	1.11	0.5	0.32	0.001	**0.40**	Bal.

After casting, heat treatment was performed at 520 °C with various holding times up to 24 h, followed by water quench to evaluate the dispersoid formation. Subsequently, a T7 aging treatment (200°C/5h) was applied to simulate the industrial application. Furthermore, long-term thermal exposure tests were performed at 300 °C for up to 1000 h to investigate the evolution of the microstructure and mechanical properties of experimental alloys during their service life.

The evolution of the mechanical properties was evaluated by Vickers microhardness and compression yield strength (YS) at room temperature (RT), as well as compression YS and creep resistance at 300 °C. Microhardness tests were performed on the Al matrix with a load of 10 g and dwell time of 20 s on the polished samples to study the influence of the dispersoids. The average of 15 measurements was calculated for each sample as the hardness value. The YS at both RT and 300 °C was obtained from the compression tests with a strain rate of 10^{-3} s^{-1}. Additionally, creep tests were performed under a constant compression load of 35 MPa at 300 °C. For each condition, three tests were repeated to confirm the reliability of the results.

To characterize the microstructure, optical microscopy was used to verify the formation and evolution of the intermetallics, as well as the formation and distribution of the dispersoid zone and DFZ during the heat treatment and long-term exposure processes. Deep-etching tests were also performed in 20% NaOH solution to reveal the 3-D morphology of the eutectic Si particles. To reveal the dispersoids, the samples were etched in 0.25% hydrofluoric acid (HF) for 90 s. Additionally, the dark-field mode on the optical microscope was used to better present the dispersoids. An SEM and a TEM equipped with an energy dispersive X-ray spectrometer (EDS) were used to observe the evolution of the dispersoids and precipitates in detail.

3. Results and discussion

3.1 As-cast microstructures of the experimental alloys

Fig. 1 shows the as-cast microstructures of the experimental alloys, which contain the α-Al dendrites, eutectic silicon, primary Mg_2Si (dark), and Al-Fe-Ni intermetallic (gray). However, several differences were observed among the alloys, especially in those with higher Mo contents (e. g. Alloys B2 and B3).

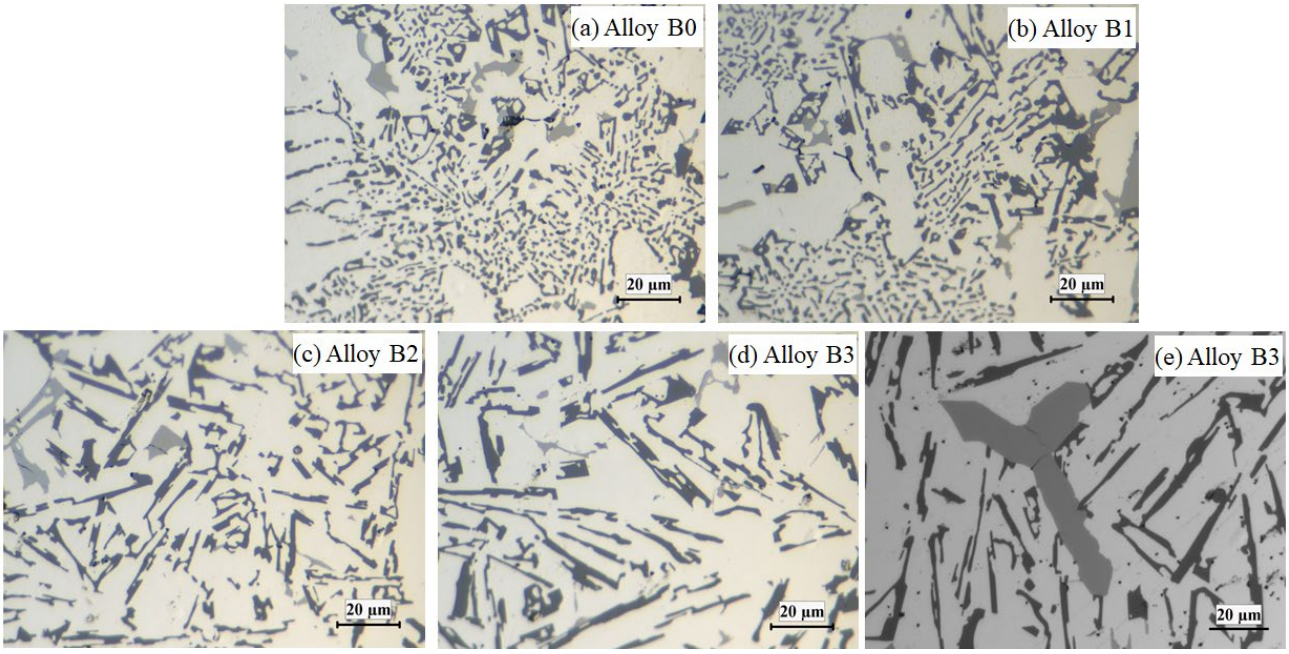

Fig. 1 As-cast microstructures of the experimental alloys

Firstly, it can be observed that the morphologies of the Si particles varied with the amount of Mo added. As shown in Fig. 1a and 1b, the eutectic Si particles in the base Alloy B0 and Alloy B1 with lower Mo content (0.15%) were mainly fine with occasional blocky plate-like Si particles, characterized by a lower aspect ratio and smaller average length (Table 2). However, the coarse plate-like Si particles became more apparent with increasing Mo content. As shown in Fig. 1c, a high fraction of the plate-like Si particles combined with a very small fraction of fine Si particles can be observed in Alloy B2 with 0.25% Mo, while approximately all Si particles changed into plate-like morphologies in Alloy B3 with 0.4% Mo (Fig. 1d). The characterization results of Si particles in Table 2 also confirm that the Mo addition changed the morphology of the Si particles by increasing the aspect ratio and average length. The aspect ratio and average length of Alloy B3 was 3 and 4.4 times greater, respectively, than that of Alloy B0. The possible reason for these changes in morphology induced by Mo may be related to the disruption of eutectic Si nucleation during solidification. However, the exact mechanism needs to be further studied.

Secondly, the primary blocky Al-Mo intermetallic was observed in Alloys B2 and B3 (Fig. 1e), and its area fraction increased with the amount of Mo added (Table 2), which can be attributed to the lower solubility of Mo in the Al matrix. The area fraction of the primary Al-Mo phase increased from 0 in Alloy B1 to 0.17% in Alloy B2 and further to 0.78% in Alloy B3.

Table 2 Characterization on the as-cast microstructure of experimental alloys

Alloy #	Eutectic Si		Area fraction of primary Al-Mo particles, %
	Aspect ratio	Average length, μm	
B0	2.3 ± 0.5	3.6 ± 1.0	0
B1	3.4 ± 0.7	4.4 ± 1.3	0
B2	6.7 ± 2.3	15.4 ± 4.6	0.17 ± 0.09
B3	7.0 ± 2.1	16.0 ± 4.0	0.78 ± 0.21

3.2 Evolution of dispersoids during heat treatment at 520 °C

According to our previous study on the formation temperature of dispersoids (~500 °C) [3] and the traditional solution treatment of Al-13%Si piston alloys at 500–560 °C [23, 24], the heat treatment at 520 °C was employed in this work to study the evolution of dispersoids. As an indicator of dispersoids precipitation, the evolution of hardness during heat treatment for all four experimental alloys is plotted in Fig. 2. Generally, the microhardness increased with time for all experimental alloys until 12 h, and then plateaued, confirming the precipitation of dispersoids. However, the microhardness of the Mo-containing alloys (Alloys B1, B2, and B3) was always higher than that of the base alloy B0, and the difference between them became increasingly larger with increasing Mo contents, indicating the different precipitation behavior of dispersoids with Mo addition.

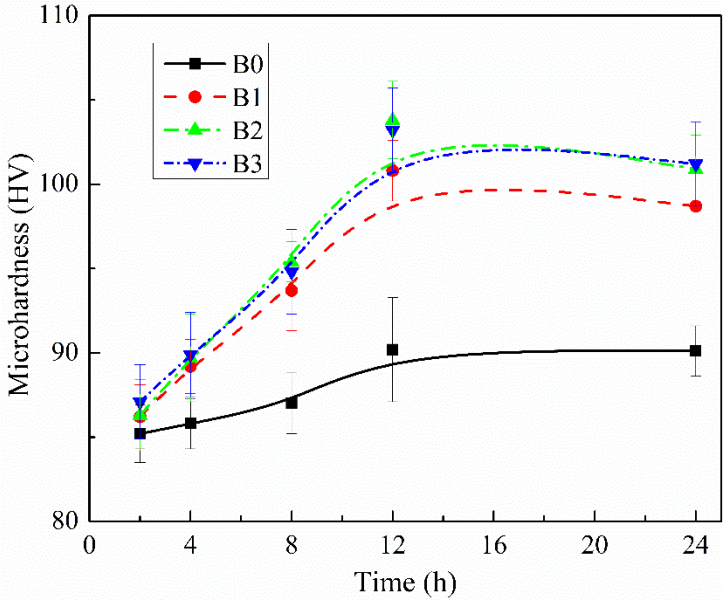

Fig. 2 Evolution of microhardness during 520 °C heat treatment

As shown in Fig. 2, the microhardness reached the peak at 520°C/12h in each of the four experimental alloys. Therefore, the microstructures of the experimental alloys under 520°C/12h were selectively observed using the dark-field mode of the OM after etching with HF solution and shown in Fig. 3. The dispersoid zone and DFZ can be clearly observed in the four experimental alloys but their characters, such as the density of dispersoids in the dispersoid zone and the area fraction of the DFZ,

varied among the alloys. In base alloy B0 (Fig. 3a), a small volume of dispersoids was sparsely distributed in the dendrite cells, and the DFZ was of relatively high volume (~32%), which explaining the slightly increase on microhardness in base alloy. In Alloy B1 with 0.15% Mo (Fig. 3b), the dispersoid zone appeared to expand with a higher density of dispersoids, and the DFZ was greatly confined to limited areas, which was more evident in Alloys B2 and B3 (Fig. 3c and 3d). As shown in Fig. 3c, a significantly larger number of dispersoids were distributed in the dendrite cells of Alloy B2, and a very low volume DFZ was observed (~8%). Therefore, the enhanced precipitation of dispersoids in the expanded dispersoid zone and the restriction of the DFZ by the Mo additions led to the higher microhardness and the increased difference on hardness with base alloy, as shown in Fig. 2. Meanwhile, similar microstructures were observed in Alloys B2 and B3 (Fig. 3c and 3d, respectively). This explains their similar tendency on microhardness, as shown in Fig. 2, which are attributed to the similar supersaturated Mo levels in the solid solutions of both alloys. Though more Mo was added to Alloy B3 (0.4%), they formed the additional Al-Mo primary phase (Table 2) instead of further increasing the Mo in the solid solution of the Al matrix during solidification.

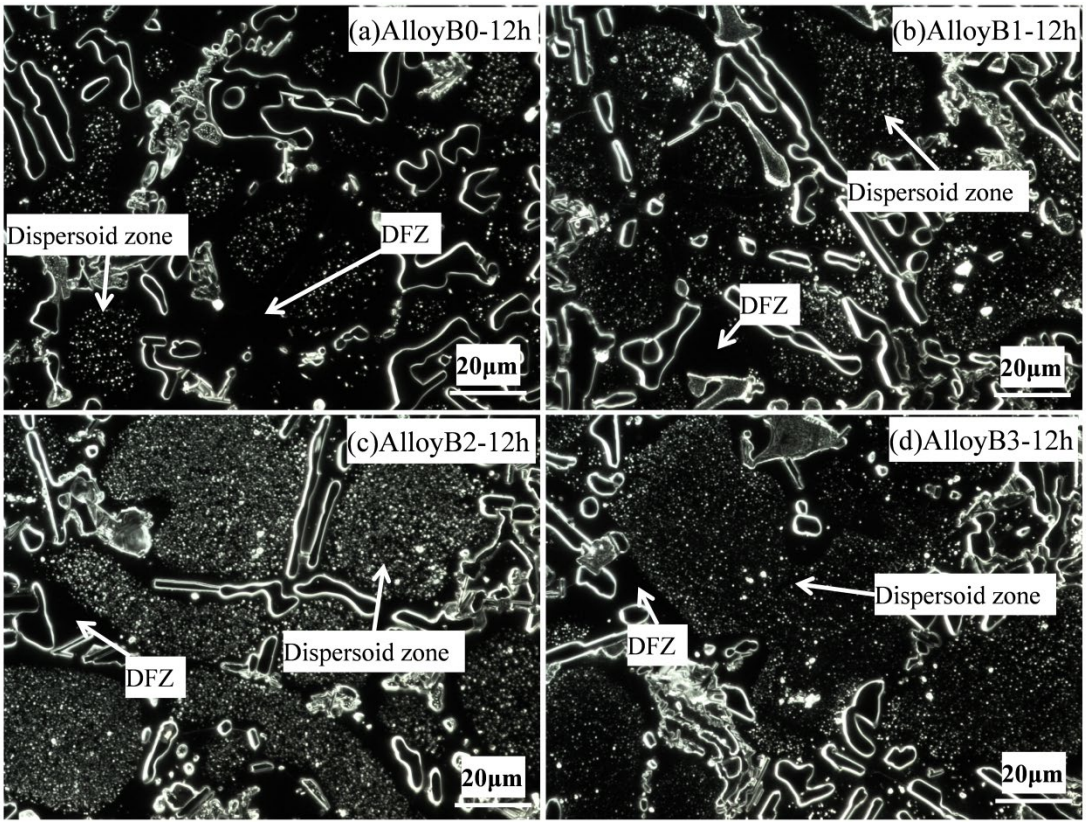

Fig. 3 Dark-field OM microstructures after heat treatment at 520°C/12h:
(a) B0, (b) B1, (c) B2, and (d) B3.

Fig. 4 shows the distribution of dispersoids in the dispersoid zone after 520°C/12h of Alloys B0 and B2 in bright-filed TEM, as well as their TEM-EDS results. The dispersoids were detected as α-Al(Mn,Fe)Si in Alloy B0 and α-Al(Mn,Mo,Fe)Si in the Mo-containing alloys (e.g., Alloy B2), as Mo

can replace Mn/Fe in the dispersoids without changing the crystallographic structure. Therefore, both of them are defined as α-dispersoids in the present work. As shown in Fig. 4, the α-dispersoids were uniformly distributed in the dispersoid zones of both alloy. However, the size and number density of dispersoids was different between Alloys B0 and B2 that the size is smaller while the number density is higher in Alloy B2 than Alloy B0, explaining the much higher microhardness in Alloy B2 in Fig. 2. The average size of α-dispersoid in Alloy B2 was measured approximately 50-70 μm with a number density of 11 um^{-3}; whereas in Alloy B0, the average size and number density was 70-90 μm and 6 um^{-3}, respectively. This indicates that the Mo addition can further improve the precipitation of α-dispersoids, which is likely due to the reverse partition coefficient of the Mn and Mo elements [25]. In brief, the precipitation of α-dispersoid in experimental alloys leads to the increase of hardness with holding time of heat treatment while the higher volume of finer α-dispersoid in alloys with Mo additions results in the increasing difference on hardness with base alloy.

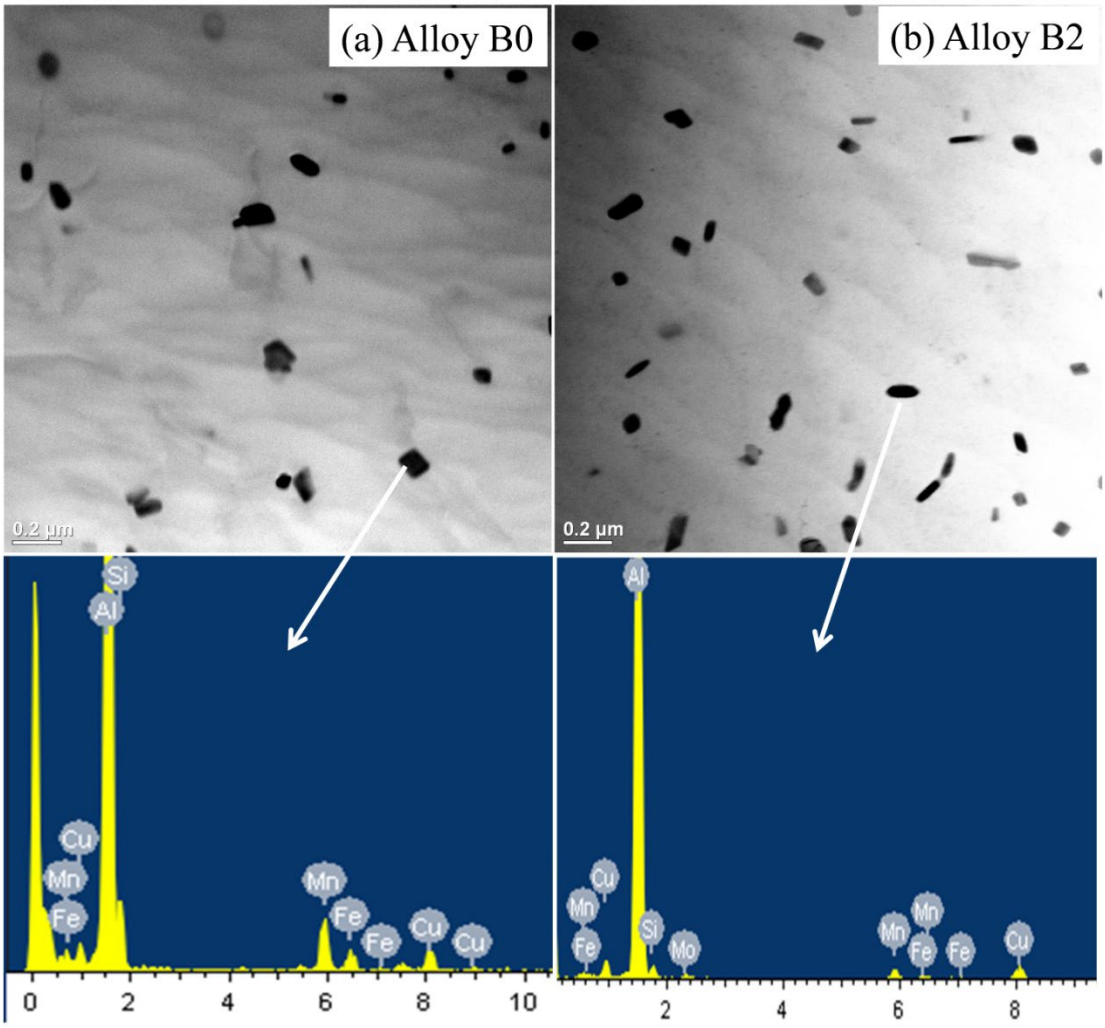

Fig. 4 TEM observations of dispersoids in the dispersoid zones and their TEM-EDS results of Alloys B0 and B2 after heat treatment at 520°C/12h

3.3 Instaneous yield strength at room and elevated temperatures

As shown in Figs. 2 and 3, the Mo addition can significantly increase the microhardness by enhancing the precipitation of dispersoids. Meanwhile, Alloy B3 exhibited similar microhardness and dispersoid behaviors to those of Alloy B2, but it contained a higher amount of coarse primary Al-Mo intermetallic. Therefore, in the present work, Alloys B0 (the base) and B2 (0.25% Mo) were selected to conduct mechanical and creep tests. Before the test, both alloys were heat treated at 520°C/12h and aged at 200°C/5h to reach the T7 condition. Subsequently, they were tested at 25 °C and 300 °C for YS and their evolution is presented in Fig. 5.

Similar to the microhardness evolution in Fig. 2, the YS at room temperature (RT) from Alloy Bo to B2 increased from 329.3 MPa to 364.8 MPa, while it increased from 152.2 MPa to 167.9 MPa at 300 °C (see Fig. 5). These increases each correspond to a 10% strength enhancement, thus confirming the improvement of the mechanical properties by adding Mo in Al-13%Si piston alloys.

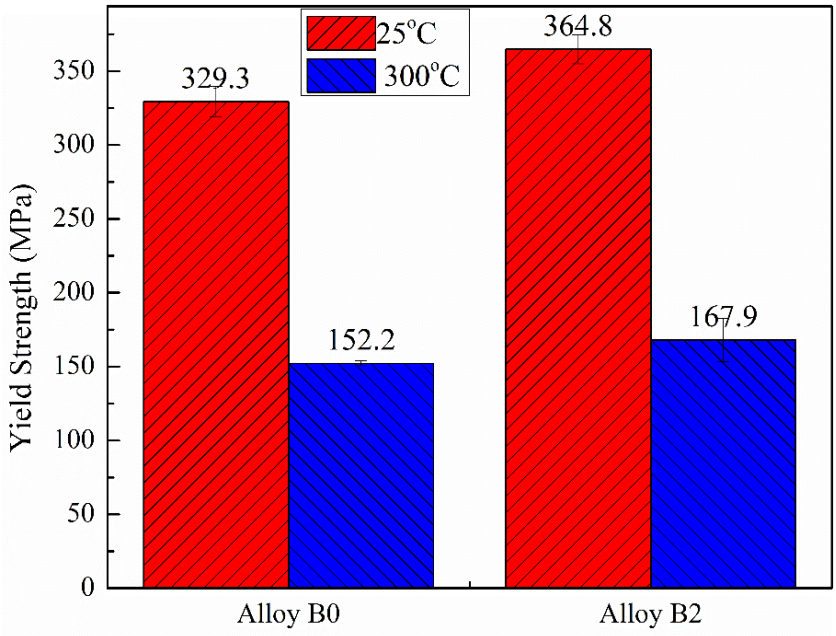

Fig. 5 Evolution of YS at 25 and 300 °C for Alloys B0 and B2 under T7

As shown in Figs. 3 and 4, the addition of Mo promoted the formation of dispersoids, leading to an increase in the microhardness (Fig. 2). However, the Si morphology partially changed from fibrous to blocky due to the Mo addition (Fig. 1), which is reported to reduce the ductility but with minimal effect on the YS [26, 27]. Therefore, it is reasonable to conclude that the increment in the instaneous YS at both RT and 300 °C in Alloy B2 can be dominantly attributed to its large volume of finer dispersoids and smaller DFZ due to the Mo addition.

3.4 Evolution of properties in service condition

As shown in Fig. 5, the increased instaneous YS at 25 and 300 °C was confirmed as a result of the Mo addition. However, the thermal stability of these mechanical properties during the service life of

Al-13% piston alloys is of particular importance. Therefore, a long-term thermal exposure at 300 °C for up to 1000h was performed to simulate service conditions in the present work. Subsequently, the stability of the mechanical properties during the service life was evaluated. The selected alloys (B0 and B2) were first T7 treated (520°C/12h + 200°C/5h) and then held at 300 °C for 100, 400, 700, and 1000h, followed by YS and creep tests at 300 °C.

Firstly, the evolutions of YS at 300 °C of Alloys B0 and B2 during thermal exposure are shown in Fig. 6. It was evident that the YS at 300°C decreased in both Alloys B0 and B2 during the thermal exposure, but the YS of Alloy B2 was always higher than that of B0. Moreover, the decline rate of YS was slower in Alloy B2 than B0. For example, the YS of Alloy B0 dropped from 64.9 MPa after 100 h to 45.4 MPa after 1000 h, corresponding to a 30% decrease. In comparison, the YS of alloy B2 only decreased from 69.5 MPa to 52.6 MPa, corresponding to a 24% decrease. Therefore, the difference in YS between the two alloys increased from 4.6 MPa after 100h to 7.2 MPa after 1000h. Therefore, it is evident that Alloy B2 has higher level of thermal stability and can resist the elevated temperature for a longer period during service. For industrial applications, it is noteworthy that the YS of alloy B2 remained approximately 7 MPa higher than that of B0 after 1000 h thermal exposure, corresponding to a 14% improvement.

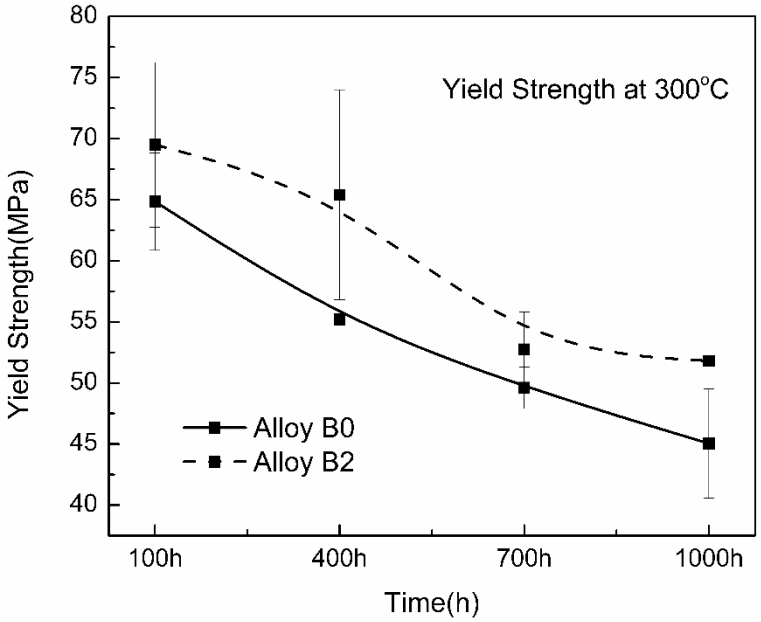

Fig. 6 Evolution of YS at 300°C for Alloys B0 and B2 during thermal exposure

Secondly, creep resistance is one of the most important criteria for high temperature applications, and it was also evaluated in the present work. Fig.7a shows the typical creep curves of Alloys B0 and B2 after 100 and 1000 h. The creep strain of both alloys was found to have increased rapidly in the first few hours during the initial stage. Then, the creep deformation turned into a quasi-steady state and the minimum creep rate was calculated at this stage. Generally, the total creep strain increased with the

holding time in both alloys. However, Alloy B2 always had a lower total creep strain under the same conditions, and the difference on the total creep strain between Alloys B2 and B0 increased with the holding time. As shown in Fig.7b, the total creep strain after 100 h, 1000h in Alloy B2 was 0.056 and 0.09, while it was higher in Alloy B0, which is 0.077 and 0.126, corresponding to a 27% and 30% improvement in creep resistance after 100 and 1000h, respectively. Meanwhile, the difference in the creep strain between the two alloys increased from 0.021 after 100 h to 0.086 after 1000 h, corresponding to a 49% enhancement in the creep resistance. In addition, the evolution of the minimum creep rate (Fig. 7b) showed a similar tendency to that of the total creep strain. While the minimum creep rate increased with the exposure time in both alloys, the increase in Alloy B2 was slower. For instance, the minimum creep rate in Alloy B0 increased from 2.1×10^{-7} after 100 h to 4.6×10^{-7} after 1000 h, which accounts to a 120% increase. In comparison, the minimum creep rate of alloy B2 increased from 1.5×10^{-7} after 100 h to 2.1×10^{-7} after 1000 h, corresponding to a moderate 40% increase, indicating a significant improvement in the creep resistance and thermal stability of Alloy B2.

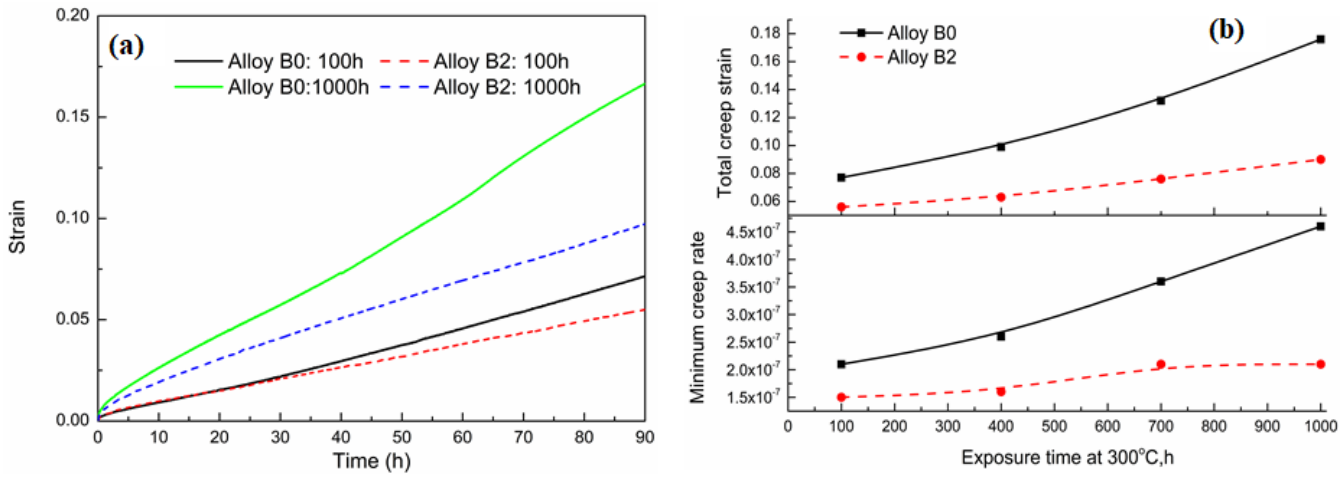

Fig. 7 (a) Typical creep curves at 300 °C and (b) evolution of creep properties during the thermal exposure of Alloys B0 and B2

As shown in Figs. 6 and 7, both the YS and creep resistance at 300 °C decreased with prolonging exposure time. However, the decline rate was slowed by the addition of Mo (e. g. Alloy B2). Two possible reasons are proposed in the present work for the deterioration of the properties, as well as the slower decline rate, in the Mo-containing alloy during long-term thermal exposure:

The first principle reason is the promoted precipitation of α-dispersoid precipitation by the Mo addition. As shown in Figs. 3 and 4, the higher volume of finer dispersoids was obtained in the Mo-containing alloys. It has been reported that α-dispersoids are thermally stable at 300-350 °C in 3xxx alloys [21, 22]), providing the stable contribution to the mechanical properties. Fig. 8 shows the TEM observation of Alloy B2 after T7 as well as after thermal exposure for 1000 h. After T7, a large number of nanoscale needle-like β'-Mg_2Si precipitates was observed in the matrix of Alloy B2 with lengths of 80-120 nm (Fig. 8a). It is evident that these fine β'-Mg_2Si precipitates provided the main strengthening

effect for the instaneous mechanical properties at both room and elevated temperatures, whereas the presence of dispersoids afforded a complementary and additional strengthening effect. During the thermal exposure, the β'-Mg_2Si precipitates were rapidly coarsened and transformed into equilibrium non-coherent β-Mg_2Si. Their size can reach 2 μm in length (Fig. 8b, indicated by black arrows), largely losing the precipitation strengthening effect, which is the principle reason for the decrease of the mechanical properties with increasing exposure time [28, 29]. However, it is noteworthy that the α-dispersoids in Alloy B2 (Fig. 8b, indicated by yellow dotted arrows) remained stable even after thermal exposure at 300°C/1000h. Their size remained in the range of 50-70 nm, which is compatible with the size of α-dispersoids just after 520°C/12h (Fig. 4b), thus confirming their perfect thermal stability during thermal exposure. Consequently, after the main strengthening phase, i.e. Mg_2Si precipitates, was coarsened and lost their strengthening effect, the dispersoid strengthening became the major strengthening mechanism at elevated temperature. Though α-dispersoids were also observed in Alloy B0 (Figs. 3a and 4a), their volume was much lower with relative bigger size compared with those of Alloy B2. Therefore, the presence of a higher volume of finer α-dispersoids in Alloy B2 provided the stable contribution to the elevated-temperature properties and then slowed the decline rate of mechanical properties.

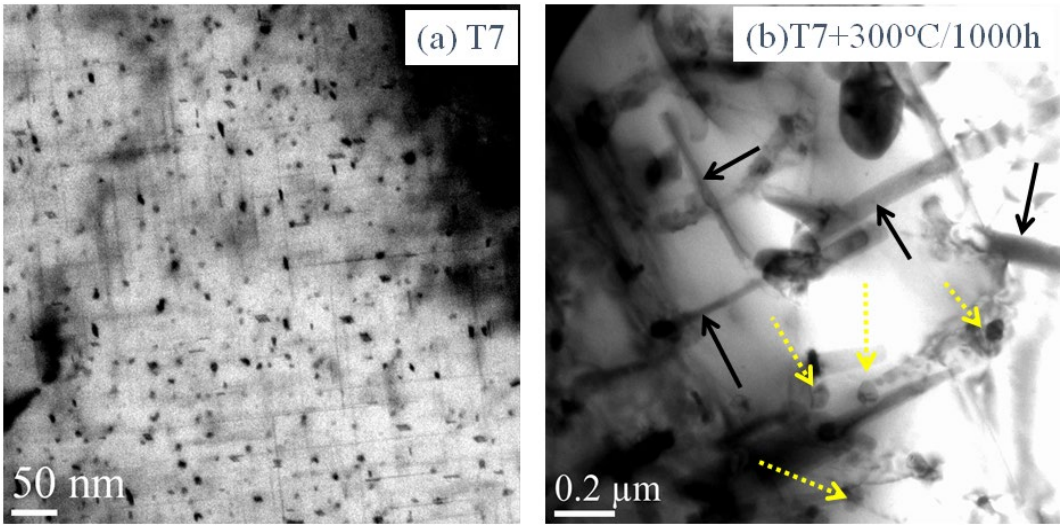

Fig. 8 TEM bright-field images of Alloy B2 under (a) T7 and (b) T7+300°C/1000h (yellow dotted arrows indicate the α-dispersoids; black arrows indicate the coarsened β-precipitates)

Another possible reason can be related to the evolution of the network during thermal exposure, in particular, the evolution of the eutectic Si morphology. It has been reported that interconnected Si particles are able to strengthen Al-13%Si piston alloys by transferring the load from the α-Al matrix to the 3-D Si network [5, 11]. Therefore, the connected Si network will be benefit to the mechanical properties during the thermal exposure. As shown in Fig. 9, the Si in Alloy B0 has been already fragmented under T7 (Fig. 9a) and continued to spheroidization during the thermal exposure [30] (Fig. 9b-c), thereby weakening the contribution of the Si network and leading to the deterioration of the

properties. However, the fragmentation and spheroidization of the Si particles has been retarded in Alloy B2, such that they were still compact platelets with only partially fragmented during the thermal exposure (Fig. 9d-f). This difference in the 3-D interactions between the Si particles is more clearly shown in Fig. 10, where it can be observed that the Si in Alloy B0 was already fragmented into fine branched particles after T7 (Fig. 10a) and continued to spheroidize during the thermal exposure (Fig. 10c). In comparison, the Si particles in Alloy B2 appeared to retain their plate-like morphology with only partial necking in certain areas (indicated by the white arrows in Fig. 10b) and without causing apparent fragmentation. After the subsequent thermal exposure to 300°C/1000h (Fig. 10d), a considerable fraction of Si particles in the Mo-containing alloy (B2) still retained their plate-like morphology, thereby retarding the fragmentation and spheroidization process of Si particles and largely restoring the Si networks in Al-13%Si alloys. Therefore, the less fragmented Si network in Alloy B2 during thermal exposure slowed the deterioration of the properties to a certain extent compared with the base alloy (B0).

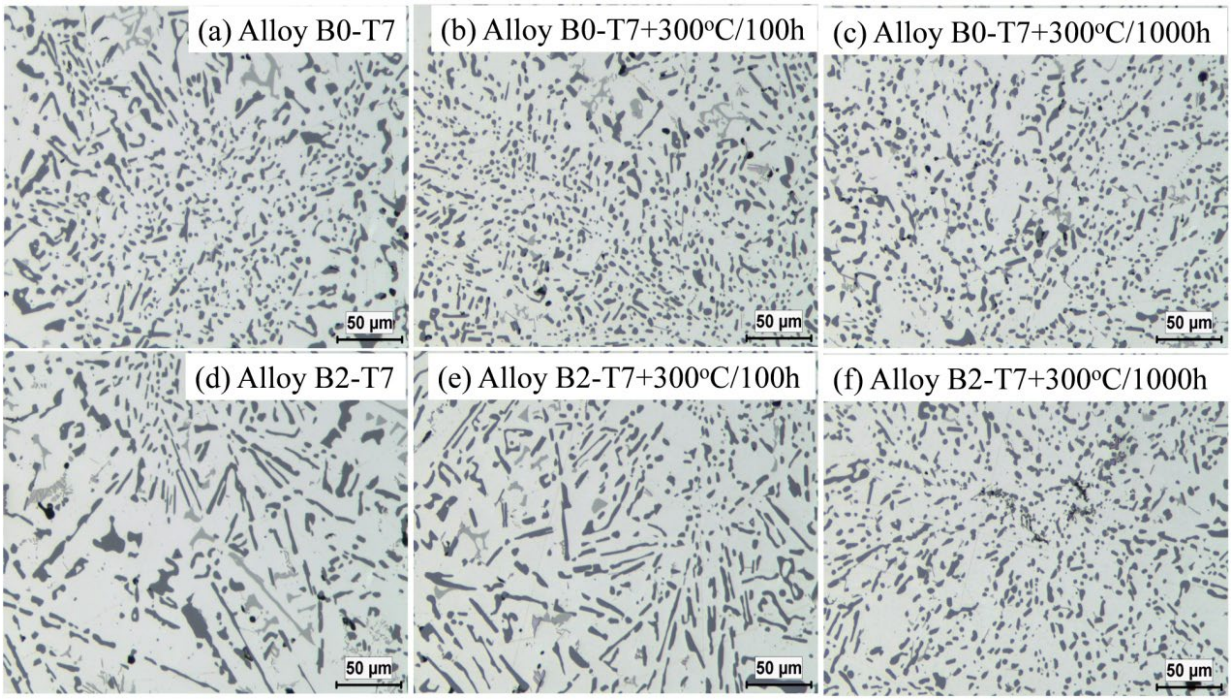

Fig. 9 Evolution of Si particles during thermal exposure in Alloys B0 and B2

Traditional heat-treatable Al-Si piston alloys are subjected to solution treatment at 500-540 °C followed by T7 artificial ageing to improve the mechanical properties at RT strengthened by the large quantity of nano-scale Mg_2Si precipitates [3]. However, the coarsening of the precipitates and deterioration of the eutectic Si network at elevated temperature restricts their strengthening effects [6]. In the present work, the Mo addition induced two factors on Al-13%Si piston alloys. First, the Mo addition promoted the precipitation of thermally stable α-dispersoids during precipitation temperature (520 °C), which is compatible with the conventional solution treatment for Al-Si piston alloys. These α-dispersoids partially compensate for the detrimental effect imposed by the coarsening of the Mg_2Si precipitates during prolonged thermal exposure. Second, the Mo addition partially changed the

morphology of Si particles and retarded their fragmentation and spheroidization during the thermal exposure, thereby slowing the deterioration of the mechanical properties. Overall, complementary strengthening of the thermally stable dispersoids in the Al matrix and retarding the Si particle spheroidization via Mo addition can provide a synergistic strengthening effect on Al-13Si piston alloys during the elevated-temperature applications.

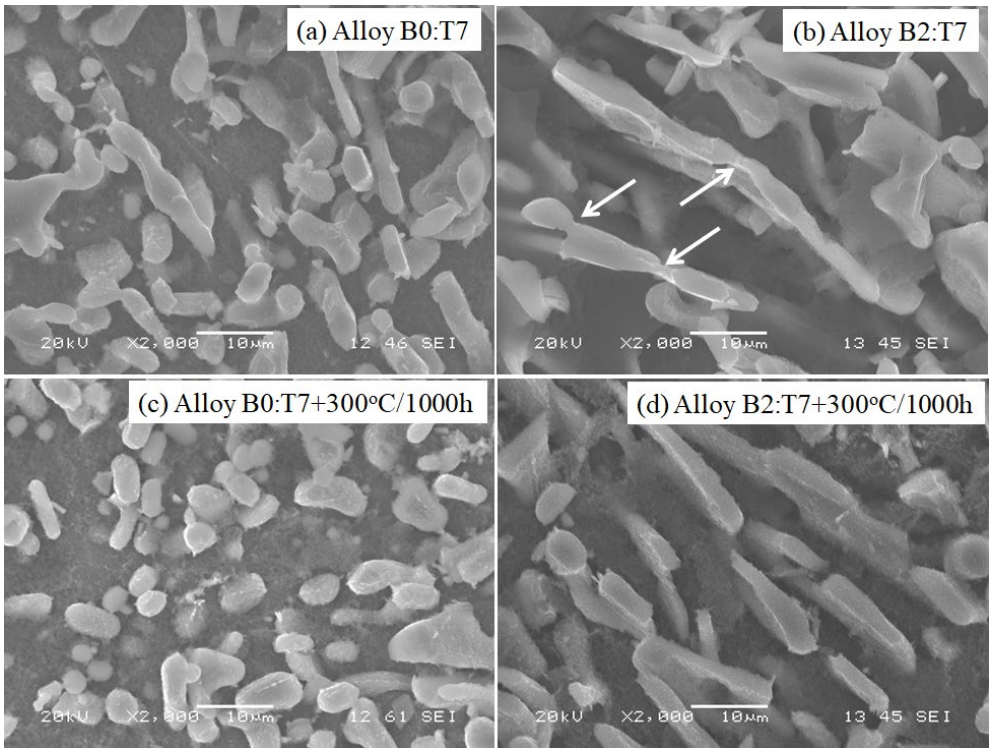

Fig. 10 3-D distribution of Si under various conditions in Alloys B0 and B2

4. Conclusions

In this study, the effects of Mo addition on the microstructure (α-dispersoids and eutectic Si), mechanical properties, and creep resistance at elevated temperature in Al-13%Si piston alloys was investigated. Based on the results, the following conclusions can be drawn:

1) Mo addition can further enhance the precipitation of α-dispersoids during heat treatment, resulting a remarkable improvement of the microhardness and the yield strength as well as the creep resistance.
2) The addition of Mo can partially change the morphology of eutectic Si particles and retard Si fragmentation and spheroidization during solution treatment and prolonged thermal exposure.
3) The coarsening of Mg_2Si precipitates and the fragmentation and spheroidization of Si particles account for the decrease in yield strength and creep resistance during the service life at elevated temperature of piston alloys.
4) The improved elevated-temperature strength and creep resistance during prolonged thermal

exposure at 300 °C in the Mo-containing alloy can be ascribed to the synergistic effect of the enhanced precipitation of thermally stable α-dispersoids and the retardation of the fragmentation and spheroidization of Si particles.

Acknowledgements

The authors would like to acknowledge the financial support from the Natural Sciences and Engineering Research Council of Canada (NSERC) and Rio Tinto Aluminum, through the NSERC Industry Research Chair in Metallurgy of Aluminum Transformation at the University of Quebec at Chicoutimi.

References

[1] M. Zeren, The effect of heat-treatment on aluminum-based piston alloys, Materials & Design 28(9) (2007) 2511-2517.

[2] Y. Wang, H. Liao, Y. Wu, J. Yang, Effect of Si content on microstructure and mechanical properties of Al–Si–Mg alloys, Materials & Design 53 (2014) 634-638.

[3] K. Liu, X.G. Chen, Improvement in elevated-temperature properties of Al-13% Si piston alloys by dispersoid strengthening via Mn addition, J Mater Res 33(20) (2018) 3430-3438.

[4] Z. Qian, X.F. Liu, D.G. Zhao, G.H. Zhang, Effects of trace Mn addition on the elevated temperature tensile strength and microstructure of a low-iron Al-Si piston alloy, Materials Letters 62(14) (2008) 2146-2149.

[5] Z. Asghar, G. Requena, E. Boller, Three-dimensional rigid multiphase networks providing high-temperature strength to cast AlSi10Cu5Ni1-2 piston alloys, Acta Materialia 59(16) (2011) 6420-6432.

[6] Z. Asghar, G. Requena, F. Kubel, The role of Ni and Fe aluminides on the elevated temperature strength of an AlSi12 alloy, Materials Science and Engineering: A 527(21) (2010) 5691-5698.

[7] V. Abouei, H. Saghafian, S.G. Shabestari, M. Zarghami, Effect of Fe-rich intermetallics on the wear behavior of eutectic Al-Si piston alloy (LM13), Materials & Design 31(7) (2010) 3518-3524.

[8] J. Feng, B. Ye, L. Zuo, R. Qi, Q. Wang, H. Jiang, R. Huang, W. Ding, Effects of Ni content on low cycle fatigue and mechanical properties of Al-12Si-0.9Cu-0.8Mg-xNi at 350°C, Materials Science and Engineering: A 706 (2017) 27-37.

[9] Y. Yang, K.L. Yu, Y.G. Li, D.G. Zhao, X.F. Liu, Evolution of nickel-rich phases in Al-Si-Cu-Ni-Mg piston alloys with different Cu additions, Materials & Design 33 (2012) 220-225.

[10] Z. Asghar, G. Requena, G.H. Zahid, D. Rafi ud, Effect of thermally stable Cu- and Mg-rich aluminides on the high temperature strength of an AlSi12CuMgNi alloy, Materials Characterization 88 (2014) 80-85.

[11] G. Requena, G. Garcés, M. Rodríguez, T. Pirling, P. Cloetens, 3D architecture and load partition in eutectic Al-Si alloys, Adv Eng Mater 11(12) (2009) 1007-1014.

[12] S.G. Shabestari, R. Gholizadeh, Assessment of intermetallic compound formation during solidification of Al-Si piston alloys through thermal analysis technique, Mater. Sci. Technol. 28(2) (2012) 156-164.

[13] R. Fernandez-Gutierrez, G.C. Requena, The effect of spheroidisation heat treatment on the creep resistance of a cast AlSi12CuMgNi piston alloy, Mater. Sci. Eng. A-Struct. Mater. Prop. Microstruct. Process. 598 (2014) 147-153.

[14] V. Páramo, R. Colás, E. Velasco, S. Valtierra, Spheroidization of the Al-Si eutectic in a cast aluminum alloy, J. of Materi Eng and Perform 9(6) (2000) 616-622.

[15] E. Arzt, E. Gohring, A model for dispersion strengthening of ordered intermetallics at high temperatures, Acta Materialia 46(18) (1998) 6575-6584.

[16] H. Liao, Y. Tang, X. Suo, G. Li, Y. Hu, U.S. Dixit, P. Petrov, Dispersoid particles precipitated during the solutionizing course of Al-12wt%Si-4wt%Cu-1.2wt%Mn alloy and their influence on high temperature strength, Materials Science and Engineering: A 699 (2017) 201-209.

[17] G. Han, W.Z. Zhang, G.H. Zhang, Z.J. Peng, Y.J. Wang, High-temperature mechanical properties and fracture mechanisms of Al-Si piston alloy reinforced with in situ TiB2 particles, Mater. Sci. Eng. A-Struct. Mater. Prop. Microstruct. Process. 633 (2015) 161-168.

[18] A.R. Farkoosh, X.G. Chen, M. Pekguleryuz, Dispersoid strengthening of a high temperature Al-Si-Cu-Mg alloy via Mo addition, Mater. Sci. Eng. A-Struct. Mater. Prop. Microstruct. Process. 620 (2015) 181-189.

[19] M. Tocci, R. Donnini, G. Angella, A. Pola, Effect of Cr and Mn addition and heat treatment on AlSi3Mg casting alloy, Materials Characterization 123 (2017) 75-82.

[20] R. Chen, Q. Xu, Z. Jia, B. Liu, Precipitation behavior and hardening effects of Si-containing dispersoids in Al–7Si–Mg alloy during solution treatment, Materials & Design 90 (2016) 1059-1068.

[21] K. Liu, X.G. Chen, Development of Al–Mn–Mg 3004 alloy for applications at elevated temperature via dispersoid strengthening, Mater. Des. 84 (2015) 340-350.

[22] K. Liu, H. Ma, X.G. Chen, Enhanced elevated-temperature properties via Mo addition in Al-Mn-Mg 3004 alloy, J. Alloys Compd. 694 (2017) 354-365.

[23] Z. Jiaqing, L. Ya, P. Haoping, W. Jianhua, S. Xuping, Spheroidization of Si in Al–12.6wt.%Si at eutectic temperature and its tensile properties, Materials Research Express 4(10) (2017) 106505.

[24] J. Wang, J. Zhu, Y. Liu, H. Peng, X. Su, Effect of spheroidization of eutectic Si on mechanical properties of eutectic Al–Si alloys, J Mater Res 33(12) (2018) 1773-1781.

[25] A.R. Farkoosh, X. Grant Chen, M. Pekguleryuz, Interaction between molybdenum and manganese to form effective dispersoids in an Al–Si–Cu–Mg alloy and their influence on creep resistance, Materials Science and Engineering: A 627 (2015) 127-138.

[26] N. Fat-Halla, Structural modification of Al-Si eutectic alloy by Sr and its effect on tensile and fracture characteristics, Journal of Materials Science 24(7) (1989) 2488-2492.

[27] F.J. Tavitas-Medrano, J.E. Gruzleski, F.H. Samuel, S. Valtierra, H.W. Doty, Effect of Mg and Sr-modification on the mechanical properties of 319-type aluminum cast alloys subjected to artificial aging, Materials Science and Engineering: A 480(1) (2008) 356-364.

[28] F. Stadler, H. Antrekowitsch, W. Fragner, H. Kaufmann, P.J. Uggowitzer, Effect of main alloying elements on strength of Al–Si foundry alloys at elevated temperatures, Int J Cast Metal Res 25(4) (2012) 215-224.

[29] L. Tian, Y. Guo, J. Li, J. Wang, H. Duan, F. Xia, M. Liang, Elevated re-aging of a piston aluminium alloy and effect on the microstructure and mechanical properties, Materials Science and

Engineering: A 738 (2018) 375-379.

[30] R. Sharma, A. Kumar, D.K. Dwivedi, Influence of Solution Temperature on Microstructure and Mechanical Properties of Two Cast Al–Si Alloys, Mater Manuf Process 21(3) (2006) 309-314.